

NANO EXPRESS

Open Access



Electronic Properties of a New All-Inorganic Perovskite TlPbI_3 Simulated by the First Principles

Zhao Liu¹, Ting Zhang¹, Yafei Wang¹, Chenyun Wang¹, Peng Zhang¹, Hojjatollah Sarvari², Zhi Chen^{2*} and Shibin Li^{1*}

Abstract

All-inorganic perovskites have been recognized as promising photovoltaic materials. We simulated the perovskite material of TlPbI_3 using ab initio electronic structure calculations. The band gap of 1.33 eV is extremely close to the theoretical optimum value. Compared TlPbI_3 with CsPbI_3 , the total energy (−3980 eV) of the former is much lower than the latter. The partial density of states (PDOS) of TlPbI_3 shows that a strong bond exists between Tl and I, resulting in the lower total energy and more stable existence than CsPbI_3 .

Keywords: All-inorganic perovskite, TlPbI_3 , CsPbI_3 , First principles

Background

Hybrid organic–inorganic halide perovskites ABX_3 (A is an organic cation, B is Pb or Sn, and X is a halide) have been widely used as solar cells and attracted enormous interest due to the low-cost and simple solution process for extensive production in the field of photovoltaic (PV) applications. The rapid rise of hybrid organic–inorganic perovskite solar cells has seen photoelectric conversion efficiencies rise from 3.8% [1] to 21.1% [2] in less than 6 years, although the fact that the perovskite absorber layers are subject to degradation because of heat and humidity. To overcome these issues, numerous investigations on enhancing the efficiency [3, 4] and long-term stability [5, 6] have been performed for years [7–12], and now, the perovskite with all-inorganic structure is a primary focus [13]. For solar cells, an appropriate band gap will give a satisfactory efficiency. And the band gap should be narrow enough to absorb a broad solar spectrum from near infrared to visible light. The open-circuit voltage V_{oc} is always lower than the band gap energy because thermodynamic detailed balance requires

the cell to be in equilibrium with its environment, which indicates that there is spontaneous light emission from the cell. Considering the two factors, the cubic cesium lead iodide (CsPbI_3) is a promising candidate for PV devices. Reference [14] reported the maximum efficiency occurs for a semiconductor with a band gap of 1.34 eV and is 33.7%.

The outer electron configuration of the thallium atom is $[\text{Xe}]4f^{14}5d^{10}6s^26p^1$, which has two valence states of +1 and +3, +1 valence compounds are more stable than +3 [15]. In this paper, we simulated the perovskite material of TlPbI_3 with a band gap of 1.33 eV using ab initio electronic structure calculations based on the Density Functional Theory (DFT), and the band gap is extremely closer to the theoretical optimum value than CsPbI_3 (Figs. 1 and 2). Compared TlPbI_3 with CsPbI_3 , the total energy (−3980 eV) of the former is much lower than the latter. The partial density of states (PDOS) of TlPbI_3 shows that a strong bond exists between Tl and I, resulting in the lower total energy and more stable existence than CsPbI_3 . Besides, we calculated the carrier concentration and found both the two materials indicate similar carrier concentration ranged from −20 to 50 °C.

Methods

We employed ab initio electronic structure calculations with DFT and the generalized gradient approximation

* Correspondence: zhichen@engr.uky.edu; shibinli@uestc.edu.cn

²Department of Electrical & Computer Engineering and Center for Nanoscale Science and Engineering, University of Kentucky, Lexington, KY 40506, USA

¹State Key Laboratory of Electronic Thin Films and Integrated Devices, School of Optoelectronic Information, University of Electronic Science and Technology of China (UESTC), Chengdu, Sichuan 610054, China

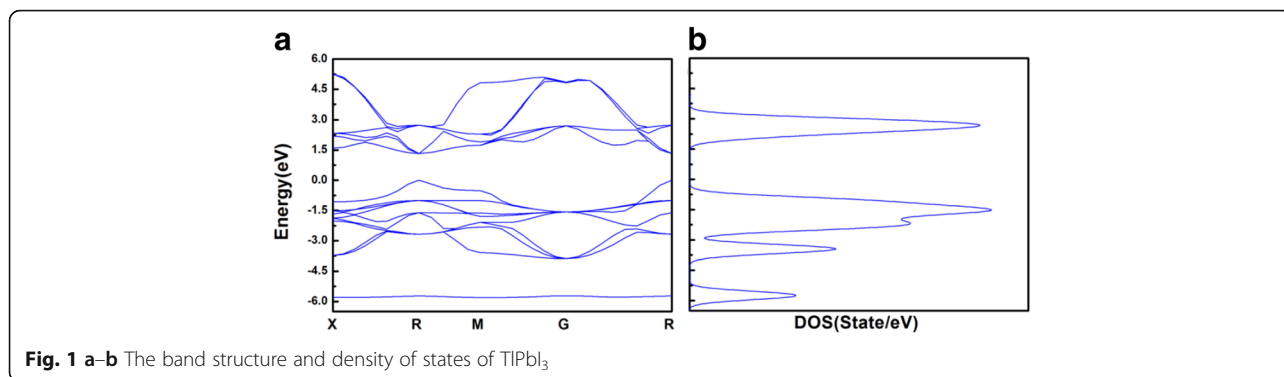


Fig. 1 a–b The band structure and density of states of TIPbl₃

(GGA) [16] put forward by Perdew–Burke–Ernzerhof (PBE) [17]. We used plane-wave basis sets and pseudo-potentials. Kohn and Hohenberg [18] suggested that the real density of electrons would lead to a quite tiny functional value. Thus, Shan and Kohn optimized and put forward the density functional theory again, namely Kohn–Sham equations (KS equation) [19]:

$$\left[-\frac{1}{2}\nabla^2 + v_{\text{ext}}(\vec{r}) + v_{\text{H}}(\vec{r}) + v_{\text{xc}}(\vec{r}) \right] \phi_i = \varepsilon_i \phi_i \tag{1}$$

Formula (1) represents the motion of the electrons in the molecular system. Where, $v_{\text{ext}}(\vec{r}) = -\sum_{\alpha=1}^N \frac{Z_{\alpha}}{|\vec{r}-\vec{r}_{\alpha}|}$ is the interaction between electrons and atoms, namely external potential. $v_{\text{H}}(\vec{r}) = \int \frac{\rho(\vec{r}')}{|\vec{r}-\vec{r}'|} d\vec{r}'$ stands for the interaction potential between electrons. $v_{\text{xc}}(\vec{r})$ is the functional differential of exchange–correlation energy. $E_{\text{xc}}, \frac{v_{\text{xc}}(\vec{r})=\delta E_{\text{xc}}[\rho(\vec{r})]}{\delta \rho(\vec{r})}$ represents the exchange–correlation potential. The effective potential $v_{\text{eff}} = v_{\text{xtf}} + v_{\text{H}} + v_{\text{xc}}$ is mainly determined by electron density, which can be obtained by KS equation. Obviously, the equation can be solved by self-consistent field equations

(SCF) if we know the exchange–correlation energy E_{xc} . After obtaining the self-consistent convergence charge density ρ_0 , the ground-state energy of the system can be expressed as [20]:

$$E_0 = \sum_{i=1}^N \varepsilon_i - \frac{1}{2} \int \int \frac{\rho_0(\vec{r}')\rho_0(\vec{r}'')}{|\vec{r}'-\vec{r}''|} d\vec{r}' d\vec{r}'' - \int v_{\text{xc}}(\vec{r})\rho_0(\vec{r}) d\vec{r} + E_{\text{xc}}[\rho_0(\vec{r})] \tag{2}$$

ε_i is the eigenvalue of Eq (1):

$$\varepsilon_i = \left\langle \phi_i \left| -\frac{1}{2}\nabla^2 + v_{\text{eff}} \right| \phi_i \right\rangle \tag{3}$$

In theory, the KS equation derived from DFT should be accurate [21]. But in the specific case, as E_{xc} is a function associated with the single electron density $\rho(\vec{r})$, it is necessary to find a function that can replace the single electron density. We can solve a set of ϕ_i by taking v_{xc} into the KS equation. Then a new v_{xc} can be calculated with this ϕ_i . Finally, we submit it into KS equation and solve. Repeat the iteration until a certain accuracy. The key problem is to find the appropriate exchange correlation energy E_{xc} . In the case of different calculation methods of exchange correlation energy E_{xc} , a series of DFT models have been reported [22]. The GGA method is more accurate because it has been combined with

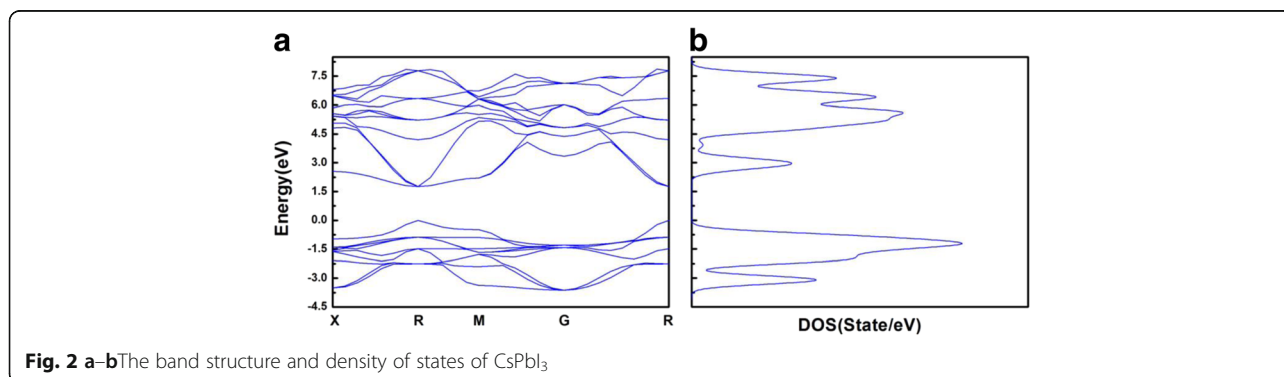


Fig. 2 a–b The band structure and density of states of CsPbl₃

inhomogeneous electron gas to obtain $E_{x,B88}$, $E_{x,LYP}$ and other parameters [23].

To calculate out carrier concentration, we must know the effective mass of electron, expressed by the following formula [18].

$$m_e^* = \hbar^2 \left[\frac{d^2 E}{dk^2} \right]^{-1} \tag{4}$$

As expressed in formula (4), effective mass of holes and electrons can be obtained by calculating the two derivatives of valence-band maximum and conduction-band bottom. Finally, the carrier concentration is obtained as follows:

$$n_i = (2.510 \times 10^{19}) \left(\frac{m_n^*}{m_0} \cdot \frac{m_p^*}{m_0} \right)^{\frac{3}{4}} \left(\frac{T}{300} \right)^{\frac{3}{2}} e^{\frac{-E_g}{2T}} \tag{5}$$

$\frac{m_n^*}{m_0}$ is the effective mass of electron, obtained by:

$$\frac{m_n^*}{m_0} = \frac{\left(\frac{6.626 \times 10^{-34}}{a \times 10^{-10}} \right)^2}{X_0 \times 1.6 \times 10^{-19} \times 9.109 \times 10^{-31}} \tag{6}$$

of which, X_0 is the two derivatives of conduction-band bottom. a is the lattice constant. Instead of conduction-band bottom by valence-band maximum, the formula (6) is often applied to solve the effective mass of hole $\frac{m_p^*}{m_0}$ [24].

The Brillouin zone was sampled with a $2 \times 2 \times 2$ k-point set and built by $2 \times 2 \times 2$ supercell. The simulated models using $6s^2 4f^{14} 5d^{10}$ and $5s^2 4d^{10} 5p^6$ as valence electrons for Tl and Cs, respectively, are carried out. Firstly, we use the ultrasoft pseudopotentials to optimize the Pm3m structures of both TlPbI₃ and CsPbI₃. Then, we calculate the equilibrium volume and proper values of the lattice constants. After optimizing the crystalline structure, we calculate the total energy, band structure, density of states, and carrier concentration for two kinds of materials in the last.

Table 1 The bond distances and bond angles of TlPbI₃ and CsPbI₃

	X = Tl	X = Cs
X-Pb	5.423 Å	5.475 Å
X-I	4.428 Å	4.471 Å
Pb-I	3.131 Å	3.161 Å
X-Pb-I	54.7361	54.7361

Results and Discussion

Optimizing the geometry of TlPbI₃ and CsPbI₃, we have simulated that the lattice constants are 6.2621 Å and 6.3225 Å, respectively. The bond distances and bond angles calculated are presented in Table 1.

The total energies of TlPbI₃ and CsPbI₃ are -3979.94 - 3154.36 eV independently. The lower total energy means the better stability. Thus, a conclusion that TlPbI₃ has better stability than CsPbI₃ is summarized theoretically.

The band gap of both semiconductors are calculated out 1.763 and 1.331 eV, respectively. The absorption spectrum of CsPbI₃ measured by the experiment (Fig. 3a) shows the optical band gap is 1.73 eV, which is close to the simulated value. And the absorption decreases above the wavelength of ~716 nm. The outcomes further indicate that the model we simulated are correct. Both of their Fermi levels are extremely close to the valence-band maximum, meaning that they are p-type semiconductors. The band gap of TlPbI₃ is quite close to the perfect semiconductor reported in reference [14]. If we can fabricate the solar cells with this material, a high efficiency will be obtained. However, the devices based on TlPbI₃ are limited to simulate because of the toxicity.

Here, we select the valence-band maximum and conduction-band minimum for further analysis. As shown in Fig. 3b, the curvature of energy band in TlPbI₃ is less than that in CsPbI₃. The conduction band of TlPbI₃ is relatively smooth and conducive to receive

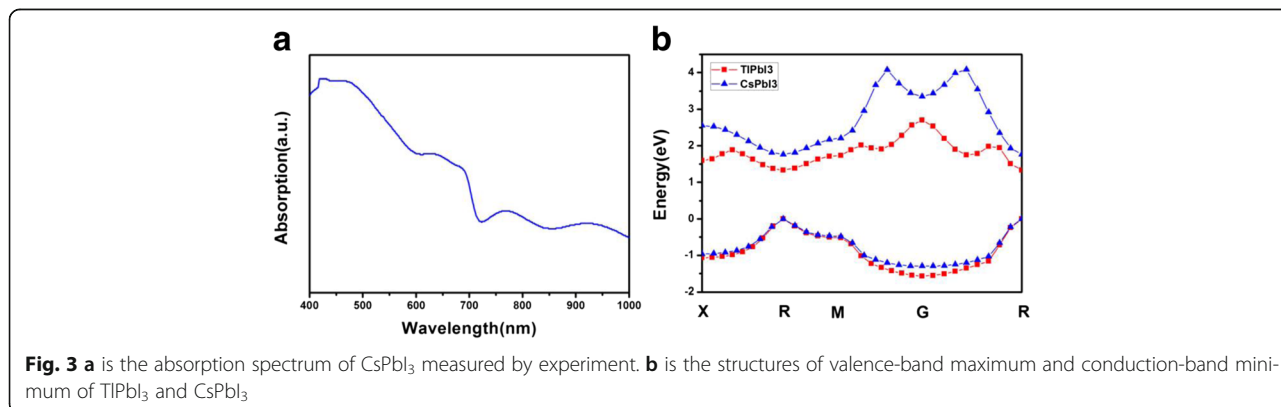
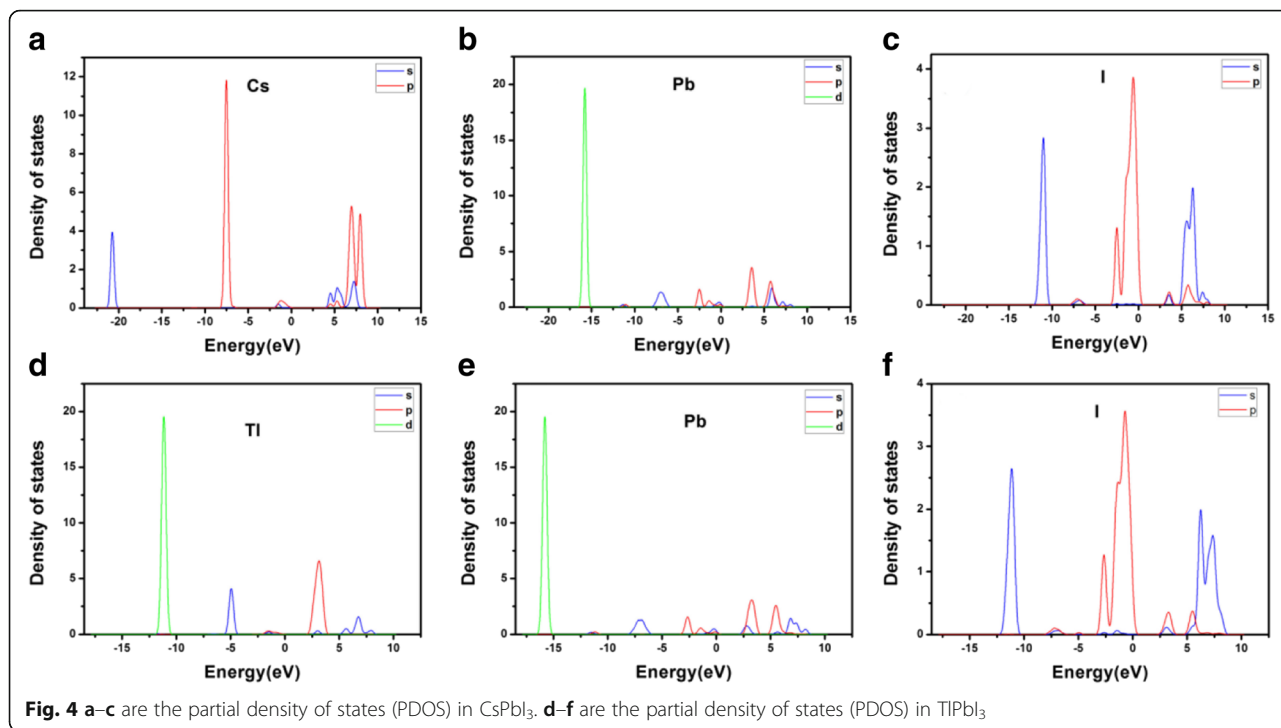


Fig. 3 a is the absorption spectrum of CsPbI₃ measured by experiment. b is the structures of valence-band maximum and conduction-band minimum of TlPbI₃ and CsPbI₃



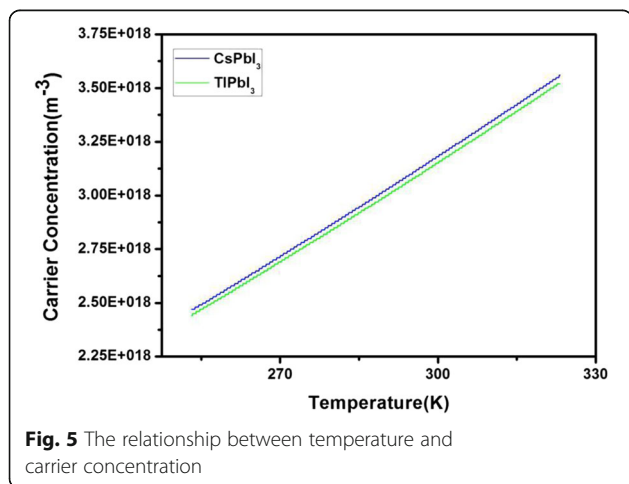
electron from valence band, enhancing the existence of carries.

According to the molecular orbital theory [25], the corresponding to the bond or anti-bond orbitals are formed by the more gentle part of the band curve. As shown in Figs. 1 and 2, if the peak of DOS curve is quite sharp, the corresponding energy-band curve is smooth; if the peak of DOS curve is relatively flat, the energy-band curve is relatively curved. So it can be deduced that the molecular orbitals are consistent with the peaks of the DOS graph. The peak height in the PDOS diagram (shown in Fig. 4) reflects the number of electrons contributing to this peak. If the PDOS of two different atoms has the resonance peaks in the range of same energy, it means the two atoms have

already bonded. However, it cannot be determined that whether the band or anti-band are formed by analyzing the PDOS without further experiments. When the existence of resonance peaks are caused by the interaction of several atoms, we cannot distinguish that the bonds are formed by the two specific atoms. The conclusion does not affect our analysis.

As illustrated in Fig. 4a–c, the conduction-band minimum of CsPbI₃ is mainly composed by 6p state of Pb, and the valence-band maximum is contributed by 5p states of I. In Fig. 4d–f, the bottom of the conduction band of TIPbI₃ is mainly composed by both 6p states of Tl and 6p states of Pb, and the top of the valence band is contributed by 5p states of I. As presented in Fig. 4d–f, Tl and I have a strong resonance peaks between –12 and –10 eV, resulting in a deep level state. It also explains why TIPbI₃ is more stable than CsPbI₃.

Finally, carrier concentration are calculated by formulas (5) and (6). The relationship between temperature and carrier concentrations of both TIPbI₃ and CsPbI₃ is shown in Fig. 5. The carrier concentration of TIPbI₃ is slightly less than that of CsPbI₃ because the electronegativity of Tl (2.04) atom is larger than that of Cs (0.79) atom [26]. A larger electronegativity leads to a larger ionic bond component and stronger polarity, enhancing the attraction between electrons.



Conclusions

We simulated the perovskite material of TIPbI₃ with a band gap of 1.33 eV using ab initio electronic structure

calculations and the band gap is extremely close to the theoretical optimum value. Compared TlPbI₃ with CsPbI₃, the total energy (−3980 eV) of the former is much lower than the latter. The partial density of states (PDOS) of TlPbI₃ shows that a strong bond exists between Tl and I, resulting in the lower total energy and more stable than CsPbI₃. Besides, we calculated the carrier concentration and found both the two materials have similar carrier concentration ranged from −20 to 50 °C.

Acknowledgements

This work was supported by the National Natural Science Foundation of China under grant nos. 61421002, 61574029, and 61371046. This work was also partially supported by the University of Kentucky.

Authors' Contributions

ZL designed and carried out the simulations. ZL and TZ participated in the work to analyze the data and prepared the manuscript initially. YW, CW, PZ, HS, ZC, and SL gave equipment support. All authors read and approved the final manuscript.

Competing Interests

The authors declare that they have no competing interests.

Publisher's Note

Springer Nature remains neutral with regard to jurisdictional claims in published maps and institutional affiliations.

Received: 28 February 2017 Accepted: 20 March 2017

Published online: 29 March 2017

References

- Kojima A, Teshima K, Shirai Y, Miyasaka T (2009) *J Am Chem Soc* 131:6050–6051
- Saliba M, Matsui T, Seo JY et al (2016) Cesium-containing triple cation perovskite solar cells: improved stability, reproducibility and high efficiency. *Energy Environ Sci* 9(6):1989–1997
- Xu QY, Yuan DX, Mu HR et al (2016) Efficiency enhancement of perovskite solar cells by pumping away the solvent of precursor film before annealing. *Nanoscale Res Lett* 11(1):248
- Zheng Y, Goh T, Fan P et al (2016) Toward efficient thick active PTB7 photovoltaic layers using diphenyl ether as a solvent additive. *ACS Appl Mater Interfaces* 8(24):15724–15731
- Ahmadian-Yazdi MR, Zabihi F, Habibi M et al (2016) Effects of process parameters on the characteristics of mixed-halide perovskite solar cells fabricated by one-step and two-step sequential coating. *Nanoscale Res Lett* 11(1):408
- Xing S, Wang H, Zheng Y et al (2016) Förster resonance energy transfer and energy cascade with a favorable small molecule in ternary polymer solar cells. *Sol Energy* 139:221–227
- Li S, Zhang P, Chen H et al (2017) Mesoporous PbI₂ assisted growth of large perovskite grains for efficient perovskite solar cells based on ZnO nanorods. *J Power Sources* 342:990–997
- Wang Y, Li S, Zhang P et al (2016) Solvent annealing of PbI₂ for the high-quality crystallization of perovskite films for solar cells with efficiencies exceeding 18%. *Nanoscale* 8(47):19654–19661
- Li H, Li S, Wang Y et al (2016) A modified sequential deposition method for fabrication of perovskite solar cells. *Sol Energy* 126:243–251
- Li S, Zhang P, Wang Y et al (2017) *Nano Res* 10:1092. doi:10.1007/s12274-016-1407-0
- Liu D, Li S, Zhang P et al (2017) Efficient planar heterojunction perovskite solar cells with Li-doped compact TiO₂ layer. *Nano Energy* 31:462–468
- Wang M, Li S, Zhang P et al (2015) A modified sequential method used to prepare high quality perovskite on ZnO nanorods. *Chem Phys Lett* 639:283–288
- Swarnkar A, Marshall A R, Sanehira E M, et al. Quantum dot-induced phase stabilization of α -CsPbI₃ perovskite for high-efficiency photovoltaics. *Science*, 2016, 354(6308): 92-95.
- Polman A, Knight M, Garnett EC et al (2016) Photovoltaic materials: present efficiencies and future challenges. *Science* 352(6283):aad4424
- Galván-Arzate S, Santamaría A (1998) Thallium toxicity. *Toxicol Lett* 99:1–13
- Perdew JP, Burke K, Ernzerhof M (1996) Generalized gradient approximation made simple. *Phys Rev Lett* 77(18):3865
- Hammer B, Hansen LB, Nørskov JK (1999) Improved adsorption energetics within density-functional theory using revised Perdew-Burke-Ernzerhof functionals. *Phys Rev B* 59(11):7413
- Hohenberg P, Kohn W (1964) Inhomogeneous electron gas. *Phys Rev* 136(3B):864
- Perdew JP, Levy M (1983) Physical content of the exact Kohn-Sham orbital energies: band gaps and derivative discontinuities. *Phys Rev Lett* 51(20):1884
- Becke AD (1993) A new mixing of Hartree-Fock and local density-functional theories. *J Chem Phys* 98(2):1372–1377
- Becke AD (1993) Density-functional thermochemistry. III. The role of exact exchange. *J Chem Phys* 98(7):5648–5652
- Hertwig RH, Koch W (1997) On the parameterization of the local correlation functional. What is Becke-3-LYP? *Chem Phys Lett* 268(5–6):345–351
- Yanai T, Tew D P, Handy N C. A new hybrid exchange–correlation functional using the Coulomb-attenuating method (CAM-B3LYP). *Chemical Physics Letters*, 2004, 393(1): 51-57.
- von Roos O (1983) Position-dependent effective masses in semiconductor theory. *Phys Rev B* 27(12):7547
- Hehre WJ (1976) Ab initio molecular orbital theory. *Acc Chem Res* 9(11):399–406
- Proud AJ, Pearson JK (2016) *Can J Chem* 94(12):1077–1081

Submit your manuscript to a SpringerOpen® journal and benefit from:

- Convenient online submission
- Rigorous peer review
- Immediate publication on acceptance
- Open access: articles freely available online
- High visibility within the field
- Retaining the copyright to your article

Submit your next manuscript at ► springeropen.com